A Physically-Consistent Bayesian Non-Parametric Mixture Model for Dynamical System Learning

Nadia Figueroa and Aude Billard
Learning Algorithms and Systems Laboratory (LASA)
École Polytechnique Fédérale de Lausanne (EPFL), Switzerland.
{nadia.figueroafernandez,aude.billard}@epfl.ch

Abstract: We propose a physically-consistent Bayesian non-parametric approach for fitting Gaussian Mixture Models (GMM) to trajectory data. Physical-consistency of the GMM is ensured by imposing a prior on the component assignments biased by a novel similarity metric that leverages locality and directionality. The resulting GMM is then used to learn globally asymptotically stable Dynamical Systems (DS) via a Linear Parameter Varying (LPV) re-formulation. The proposed DS learning scheme accurately encodes challenging nonlinear motions automatically. Finally, a data-efficient incremental learning framework is introduced that encodes a DS from batches of trajectories, while preserving global stability. Our contributions are validated on 2D datasets and a variety of tasks that involve single-target complex motions with a KUKA LWR 4+ robot arm.

Keywords: Bayesian Non-Parametrics, Side-Information, Stable Dynamical Systems

1 Introduction

Learning from Demonstration (LfD) is a paradigm that endows robots with the capabilities of learning and generalizing from observations of demonstrated tasks [1, 2, 3]. Such tasks are generally motion plans represented as mapping functions, $\mathbf{f}(\boldsymbol{\xi}) : \mathbb{R}^M \rightarrow \mathbb{R}^M$, that approximate a direct mapping from the state observations to the required actions for the demonstrated behavior; i.e. $\dot{\boldsymbol{\xi}} = \mathbf{f}(\boldsymbol{\xi})$ with $\boldsymbol{\xi} \in \mathbb{R}^M$ being the state-space variable of the robotic system. From a machine learning perspective, estimating $\mathbf{f}(\dot{\boldsymbol{\xi}})$ from data can be framed as a regression problem, where the inputs are the state variables $\boldsymbol{\xi}$ and the outputs are their first-order derivatives $\dot{\boldsymbol{\xi}}$. Several statistical methods have been proposed in the past to approximate $\mathbf{f}(\boldsymbol{\xi})$, such as Locally Weighted Projection Regression (LWPR) [4], Gaussian Processes (GPR) [5] and Gaussian Mixture Regression (GMR) [6]. Due to its intuitive nature of representing a *non-linear* regressive function as a *mixture* of linear regressors, a great body of work uses the latter statistical method (GMR) to encode motions from demonstrations. However, as discussed in [7, 8, 9], solely using any of these techniques cannot ensure convergence to a desired target. This led to researchers formulating $\mathbf{f}(\boldsymbol{\xi})$ as a first-order, autonomous Dynamical System (DS) that is *globally asymptotically stable (GAS)*; i.e. converges to a single stable equilibrium point $\boldsymbol{\xi}^*$ (a target or *attractor*)[7, 8]. To learn such *GAS*-DS from demonstrations, [8] proposed the SEDS approach, approximating $\mathbf{f}(\boldsymbol{\xi})$ as a non-linear combination (or mixture) of linear DS:

$$\dot{\boldsymbol{\xi}} = \mathbf{f}(\boldsymbol{\xi}) = \sum_{k=1}^{K} \gamma_k(\boldsymbol{\xi})(\mathbf{A}_k\boldsymbol{\xi} + \boldsymbol{b_k}) \tag{1}$$

where $\gamma_k(\boldsymbol{\xi})$ is a state-dependent mixing function. Given a set of reference trajectories $\{\boldsymbol{\Xi}, \dot{\boldsymbol{\Xi}}\} = \{\boldsymbol{\xi_t^{\text{ref}}}, \boldsymbol{\dot{\xi}_t^{\text{ref}}}\}_{t=1\dots T_N}$ SEDS parametrizes (1) via GMR. Namely, it estimates a joint density of $\{\boldsymbol{\Xi}, \dot{\boldsymbol{\Xi}}\}$ through a K-component GMM, $p(\boldsymbol{\xi}, \dot{\boldsymbol{\xi}}|\theta_\gamma) = \sum_{k=1}^{K} \pi_k \mathcal{N}(\boldsymbol{\xi}, \dot{\boldsymbol{\xi}}|\boldsymbol{\mu}^k, \boldsymbol{\Sigma}^k)$ where $\boldsymbol{\mu}^k \in \mathbb{R}^{2M}$, $\boldsymbol{\Sigma}^k \in \mathbb{R}^{2M\times 2M}$ are the mean and Covariance of each k-th component and π_k are the priors (or mixing weights) of each Gaussian component, satisfying the constraint $\sum_{k=1}^{K} \pi_k = 1$. $\theta_\gamma = \{\pi_k, \boldsymbol{\mu}^k, \boldsymbol{\Sigma}^k\}_{k=1}^{K}$ is the complete set of parameters. (1) is estimated by computing the expectation over the conditional density $\dot{\boldsymbol{\xi}} = \mathbb{E}\{p(\dot{\boldsymbol{\xi}}|\boldsymbol{\xi})\}$. Via a slight change of variables (1) is parametrized by $\gamma_k(\boldsymbol{\xi}) = \frac{\pi_k p(\boldsymbol{\xi}|k)}{\sum_j \pi_j p(\boldsymbol{\xi}|j)}$, $\mathbf{A}_k = \boldsymbol{\Sigma}^k_{\dot{\boldsymbol{\xi}}\boldsymbol{\xi}}(\boldsymbol{\Sigma}^k_{\boldsymbol{\xi}})^{-1}$, $\boldsymbol{b_k} = \boldsymbol{\mu}^k_{\dot{\boldsymbol{\xi}}} - \mathbf{A}_k\boldsymbol{\mu}^k_{\boldsymbol{\xi}}$. To ensure convergence, SEDS defines sufficient conditions for global asymptotic stability on θ_γ, namely $(\mathbf{A}_k)^T + \mathbf{A}_k \prec 0 \ \forall k = 1, \dots, K$ must hold. These conditions are derived via Lyapunov's second method for stability, which states that a DS is *GAS* at $\boldsymbol{\xi}^* \in \mathbb{R}^M$, if there exists a $\mathcal{C}^1$ Lyapunov candidate function $V(\boldsymbol{\xi}) : \mathbb{R}^M \rightarrow \mathbb{R}$ that is radially unbounded and satisfies: $(\mathbf{I})\ V(\boldsymbol{\xi}^*) = 0, (\mathbf{II}) V(\boldsymbol{\xi}) > 0 \ \forall\, \boldsymbol{\xi} \in \mathbb{R}^M \setminus \boldsymbol{\xi} = \boldsymbol{\xi}^*, (\mathbf{III})\dot{V}(\boldsymbol{\xi}^*) = 0, (\mathbf{IV})\dot{V}(\boldsymbol{\xi}) <$

2nd Conference on Robot Learning (CoRL 2018), Zürich, Switzerland.

$0 \; \forall \; \boldsymbol{\xi} \in \mathbb{R}^M \setminus \boldsymbol{\xi} = \boldsymbol{\xi}^*$. In SEDS and its latest extensions [10, 11], $V(\boldsymbol{\xi})$ is a quadratic Lyapunov function (QLF); i.e. $V(\boldsymbol{\xi}) = (\boldsymbol{\xi} - \boldsymbol{\xi}^*)^T(\boldsymbol{\xi} - \boldsymbol{\xi}^*)$. Though popular in the LfD community, SEDS is known to suffer from the *accuracy vs. stability* dilemma, i.e. it performs poorly in *highly non-linear* motions that contain high curvatures or are non-monotic (temporarily moving away from the attractor). This is mainly due to the choice of Lyapunov function; e.g. geometrically, a QLF can only allow trajectories whose L_2-norm (i.e.$||\boldsymbol{\xi} - \boldsymbol{\xi}^*||_2$) distances decrease monotonically [8, 12].

Related Work Several works have sought out to alleviate the limitations of SEDS by proposing extensions of the approach with less conservative stability conditions. [12] introduced τ-SEDS, a theoretical framework that embeds complex Lyapunov functions into the SEDS learning scheme via diffeomorphic transformations. [13] proposed CDSP (Contracting Dynamical System Primitives) in which partial contraction analysis is used to derive stability conditions. Others have tackled the problem by proposing alternatives to the SEDS-like formulation. [14] learn $\dot{\boldsymbol{\xi}} = \mathbf{f}(\boldsymbol{\xi})$ via a Neural Network (NN) and impose stability by sampling constraints, from a defined workspace, while learning the weights of the NN. [9, 15] follow a control-stabilization approach, in which an unstable DS learned via GMR (for [15]) or any other regressive algorithm (for [9]) are stabilized by a control input that is derived from either a data-driven Lyapunov function [9] or from contraction theory [15]. These approaches, however, suffer from the risk of over-corrections which might deviate the DS from the desired non-linear motion. Finally, [16] proposed an approach where $\dot{\boldsymbol{\xi}} = \mathbf{f}(\boldsymbol{\xi})$ is a diffeomorphism of a stable linear DS, which is learned via a matching algorithm from the reference trajectories to a linear motion. From the previously mentioned body of work, τ-SEDS [12], CDSP [13] and the diffeomorphic matching approach [16] have shown the best performance. Yet, they have their own drawbacks. For example, τ-SEDS and CDSP remain limited to offline batch learning settings due to the tying of the individual linear DS parameters $\mathbf{A}_k, \boldsymbol{b}_k$ to the parameters of the GMM. When optimizing θ_γ the locality and geometrical notion of the GMM wrt. reference trajectories is lost. This is an artifact that is not desirable if one seeks to exploit the generative nature of the GMM which can potentially be used for recognition or in incremental learning settings. The diffeomorphic matching approach, is also limited to offline learning, and further it can only learn a single behavior in the state-space, as the diffeomorphism is assumed to be (and learned) as a global operator. In this paper, we advocate and present an approach that:

(i) Through a simple re-formulation of the parameters of (1) is capable of outperforming SEDS using standard Lyapunov stability theory; i.e. without having to rely on diffeomorphisms or contraction analysis.

(ii) Preserves the locality of the Gaussian functions such that recognition and incremental learning is feasible.

Proposed Approach Consider (1) as a polytopic (quasi) Linear Parameter Varying (LPV) system [17]; i.e. $\mathbf{A}_k$'s, are linear time-invariant (LTI) and the state-dependent mixing function $\gamma_k(\boldsymbol{\xi})$ yields a parameter vector $\boldsymbol{\gamma} = [\gamma_1, \dots, \gamma_K]$ belonging to the convex K-unit polytope. In LTI systems parametrized QLF (P-QLF) are commonly used to ensure stability, i.e. with $V(\boldsymbol{\xi}) = (\boldsymbol{\xi} - \boldsymbol{\xi}^*)^T\mathbf{P}(\boldsymbol{\xi} - \boldsymbol{\xi}^*)$ one can ensure *GAS* of a linear DS if $\mathbf{A}^T\mathbf{P} + \mathbf{P}\mathbf{A} \prec 0$ holds, as shown in Appendix A, which can easily be extended for a mixture of linear systems (1), as shown in Appendix B. The effect of $\mathbf{P}$ is a reshaping of the simple QLF to an "elliptical" form, allowing for trajectories which exhibit high-curvatures and non-monotonicity towards the target. Solving an optimization problem for SEDS with such conditions, however, becomes unfeasible. To alleviate this, we propose to decouple the GMM parameters θ_γ from the linear DS parameters $\theta_f = \{\mathbf{A}_k, \boldsymbol{b}_k\}_{k=1}^K$, as introduced in [18, 19]; we will herein refer to this parametrization of (1) as LPV-DS. Due to this decoupling of parameters, the LPV-DS approach preserves the geometric representation of the GMM, while accurately representing highly non-linear motions due to the less conservative P-QLF. Yet, the performance of the LPV-DS approach relies heavily on a "good" estimate of the GMM parameters θ_γ. Not only must one find the correct number of Gaussians K that best represent the reference trajectories, but they should also be aligned with the trajectories such that each Gaussian represents a local region in the state space that follows a linear DS. Such an estimate is empirically hard to find, as standard EM estimation or Bayesian Non-parametric approaches, do not optimize for these properties in the data. Hence, for the LPV-DS approach to achieve comparable performance to the works mentioned above, a *physically-consistent* estimate of the GMM parameters is crucial.

Contributions We tackle two main issues involved with fitting GMM to trajectory data for accurate DS estimation: (i) **cardinality:** automatically estimating the optimal K Gaussian components (ii) **physical-consistency:** ensuring that the location and coverage of each Gaussian component corresponds to a linear DS. To solve (i) we adopt a *Bayesian non-parametric* approach. When fitting a mixture model, instead of doing model selection to find the *optimal* K, a Dirichlet process ($\mathcal{DP}$) prior (or its Chinese Restaurant Process $\mathcal{CRP}$ representation) is used to construct an infinite mixture model. In order to bias the Gaussian fitting (or clustering) of the trajectories in a physically consistent way, we propose to use a novel similarity measure based on a locally-scaled cosine

similarity of the velocity measurements of the trajectories as side-information [20]. A prior that is capable of including such side-information in a Bayesian non-parametric model is the distance-dependent $\mathcal{CRP}$ (dd-$\mathcal{CRP}$) [21]. We adopt this prior and propose a Bayesian non-parametric GMM that is biased by this measure of physical-consistency as described in Section 2. We then introduce a generalized formulation of LPV-DS with several optimization variants and prove that using our physically-consistent GMM yields improved reproduction and generalization accuracy over SEDS (Section 3). Finally, in Section 5, we propose an *incremental* approach to learning LPV-DS based on the approached proposed in Sections 3 and 2 and prove that the resulting estimate is *GAS*.

2 Physically-Consistent Bayesian Non-Parametric Mixture Model

We begin by re-interpreting the finite GMM as a hierarchical model, where each k-th mixture component is viewed as a cluster, represented by a Gaussian distribution $\mathcal{N}(\cdot|\theta_\gamma^k)$ with $\theta_\gamma^k = \{\mu_\gamma^k, \theta_\gamma^k\}$ and mixing weight π_k. Each data-point $\boldsymbol{\xi}_i$ is assigned to a cluster k via cluster assignment indicator variables $Z = \{z_1, \dots, z_M\}$, where $i : z_i = k$ for M samples. This process is represented as:

$$\begin{aligned} &z_i \in \{1, \dots, K\} \\ &p(z_i = k) = \pi_k \\ &\boldsymbol{\xi}_i | z_i = k \sim \mathcal{N}(\theta_\gamma^k) \end{aligned} \tag{2}$$

$$p(\boldsymbol{\xi}|\theta_\gamma) = \sum_{k=1}^{K} p(z_i = k)\mathcal{N}(\boldsymbol{\xi}|\boldsymbol{\mu}^k, \boldsymbol{\Sigma}^k) \tag{3}$$

Via (2), the probability density function of the mixture model is defined by (3) with $\theta_\gamma = \{\pi_k, \theta_\gamma^k\}_{k=1}^K$. In the *finite* case, since K is known *apriori* the marginal distribution over Z is solely defined by the set of mixing weights $\boldsymbol{\pi} = \{\pi_k\}_{k=1}^K$ and thus the prior probability of the cluster assignment indicator variable z_i is $p(z_i = k) = \pi_k$. In the *infinite* case, $K \to +\infty$ and all parameters are treated as latent variables by placing priors on them. The Normal-Inverse-Wishart ($\mathcal{NIW}$) distribution can be placed as a prior on the cluster parameters θ_γ^k and the $\mathcal{DP}$ is placed as a prior on the cluster assignment variables $p(Z)$. Since the $\mathcal{DP}$ is an infinite distribution over distributions, to evaluate an *infinite* mixture model on a *finite* set of samples, the Chinese Restaurant Process ($\mathcal{CRP}$) is commonly used to yield a tractable estimation of the prior $p(Z)$. The process is inspired by a culinary metaphor of a Chinese restaurant with an infinite number of tables [22]. It defines a sequence of probabilities for the incoming customers (i.e. observations $\boldsymbol{\xi}_i$) to sit at specific tables (i.e. to be assigned to a specific cluster) $p(z_i = k)$ [22]. Through inference of the $\mathcal{CRP}$-GMM one can jointly estimate the optimal number of components K and corresponding parameters θ_γ. While this solves the **cardinality** problem, L_2 distance-based approaches can perform poorly when the distribution of the points exhibits idiosyncrasies such as high curvatures, non-uniformities, etc, as shown in Figure 1. To tackle this **physical-consistency** issue, rather than using the $\mathcal{CRP}$ as a prior on $p(Z)$, we propose to use the distance-dependent $\mathcal{CRP}$ (dd-$\mathcal{CRP}$) introduced in [21], which focuses on the probability of customers sitting *with other customers* (i.e. observation $\boldsymbol{\xi}_i$ being clustered with $\boldsymbol{\xi}_j$) based on an external measure of distance. We thus reformulate the dd-$\mathcal{CRP}$ into a **physically-consistent** similarity dependent-$\mathcal{CRP}$ to bias clustering on a Bayesian non-parametric GMM with the *physically-consistent* similarity measure proposed in the following section.

2.1 Physical Consistency via $\dot{\boldsymbol{\xi}}$-Similarity

In trajectory data, there are two main properties that must hold in order for a cluster of points to be *physically consistent: (i) directionality* and *(ii) locality*. We thus propose a similarity measure composed of a locally-scaled shifted cosine similarity kernel, which we refer to as $\dot{\boldsymbol{\xi}}$-similarity,

$$\Delta_{ij}(\boldsymbol{\xi}_i, \boldsymbol{\xi}_j, \dot{\boldsymbol{\xi}}_i, \dot{\boldsymbol{\xi}}_j) = \underbrace{\left(1 + \frac{(\dot{\boldsymbol{\xi}}_i)^T \dot{\boldsymbol{\xi}}_j}{||\dot{\boldsymbol{\xi}}_i|| ||\dot{\boldsymbol{\xi}}_j||}\right)}_{\text{Directionality}} \underbrace{\exp\Big(-l||\boldsymbol{\xi}_i - \boldsymbol{\xi}_j||^2\Big)}_{\text{Locality}} \tag{4}$$

The first term measuring *directionality* is the shifted cosine similarity of pair-wise velocity measurements; i.e. $\overline{\cos}(\angle(\dot{\boldsymbol{\xi}}_i, \dot{\boldsymbol{\xi}}_j)) \in [0, 2]$ and is bounded by the angle between the pair-wise velocities $\theta_{ij} = \angle(\dot{\boldsymbol{\xi}}_i, \dot{\boldsymbol{\xi}}_j)$. When $\theta_{ij} = \pi$ (its maximum value), the velocities are in opposite direction and $\overline{\cos}(\theta_{ij}) = 0$, when $\theta_{ij} = \{\pi/2, 3\pi/2\}$ the velocities are orthogonal to each other, which yields $\overline{\cos}(\theta_{ij}) = 1$ and finally, when $\theta_{ij} = \{0, 2\pi\}$ the cosine similarity value is at its maximum $\overline{\cos}(\theta_{ij}) = 2$ as the pair-wise velocities are pointing in the same direction. This term would suffice as a measure of physical-consistency for trajectories that do not include repeating patterns, however for trajectories such as a sinusoidal wave, $\overline{\cos}(\theta_{ij})$ can yield its maximum value even if the trajectories are not close to each other in Euclidean space. Hence, to enforce *locality* we scale the $\overline{\cos}(\theta_{ij})$

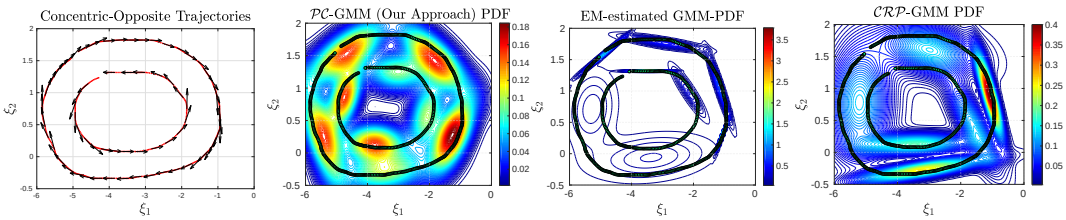

(a) Concentric Circles Dataset (b) $\mathcal{PC}$-GMM via Sampling (c) Finite GMM via EM (d) $\mathcal{CRP}$-GMM via Sampling

Figure 1: Performance of different GMM fitting strategies on *concentric* trajectory dataset. Arrows in (a) indicate velocity directions.

with a Gaussian kernel on the position measurements, i.e. the second term in (4). Notably, $l = \frac{1}{2\sigma^2}$ is a hyper-parameter that can be a nuisance if not set properly. We thus propose to set σ with the following data-driven heuristic: $\sigma = \sqrt{\text{Mo}(\mathbf{D})/2}$ where $\mathbf{D} \in \mathbb{R}^{M\times M}$ is a matrix of pairwise squared Euclidean distances $d_{ij} = ||\boldsymbol{\xi}_i - \boldsymbol{\xi}_j||^2$ and Mo is the mode of all entries of $\mathbf{D}$. Intuitively, we are approximating the *length-scale* of the trajectories. Such approximation is sufficient, as we solely use this kernel to scale high $\overline{\cos}(\theta_{ij})$ values that are 'far away' in Euclidean-position space.

2.2 $\dot{\boldsymbol{\xi}}$-Similarity Dependent-$\mathcal{CRP}$

Our physically-consistent similarity-dependent $\mathcal{CRP}$ generates a prior distribution $p(C)$ over customer seating assignments $C = \{c_1, \ldots, c_M\}$ where $i : c_i = j$ indicates that the i, j-th customers (i.e. observations $\boldsymbol{\xi}_i$ and $\boldsymbol{\xi}_j$ are clustered together based on an their $\dot{\boldsymbol{\xi}}$-similarity (4). This is done by constructing a sequence of probabilities, where the i-th customer ($\boldsymbol{\xi}_i$) has two choices, she/he can sit with the j-th customer ($\boldsymbol{\xi}_j$) with a probability proportional to (4), or sit alone with probability proportional to α. Such sequence yields a prior distribution which is a multinomial over *customer seating* assignments C conditioned on $\boldsymbol{\Delta}$ and α; i.e. $p(C|\boldsymbol{\Delta}, \alpha)$ and can be computed as,

$$p(C \mid \boldsymbol{\Delta}, \alpha) = \prod_{i=1}^{M} p(c_i = j \mid \boldsymbol{\Delta}, \alpha) \;\text{ where }\; p(c_i = j \mid \boldsymbol{\Delta}, \alpha) = \begin{cases} \frac{\Delta_{ij}(\cdot)}{\sum_{j=1}^{M} \Delta_{ij}(\cdot)+\alpha} & \text{if} \quad i \neq j \\ \frac{\alpha}{M+\alpha} & \text{if} \quad i = j \end{cases} \tag{5}$$

where $\boldsymbol{\Delta} \in \mathbb{R}^{M\times M}$ is the matrix of pairwise similarities computed by (4) between the M customers and α is the concentration parameter. We refer to this distribution as the $\dot{\boldsymbol{\xi}}$-$\mathcal{SD}$-$\mathcal{CRP}$ prior.

2.3 $\dot{\boldsymbol{\xi}}$-$\mathcal{SD}$-$\mathcal{CRP}$ Mixture Model or $\mathcal{PC}$-GMM

Using (5) and the $\mathcal{NIW}(\lambda_0)$ distribution we construct the following $\mathcal{P}$hysically-$\mathcal{C}$onsistent GMM (See Appendix C) for graphical model in (6). Where $C = \{c_1, \ldots, c_N\}$ are sampled from the $\dot{\boldsymbol{\xi}}$-$\mathcal{SD}$-$\mathcal{CRP}$ prior and then mapped to $Z = \{z_1, \ldots, z_N\}$, via a recursive mapping function $Z = \mathbf{Z}(C)$ that gathers all linked customers. For each k-th cluster, its parameters θ_γ^k are drawn from a $\mathcal{NIW}$ distribution, with hyper-parameters $\lambda_0 = \{\mu_0, \kappa_0, \Lambda_0, \nu_0\}$. The optimal number of Gaussian components K is given by the number of unique clusters that emerge from C; i.e. $K = |\mathbf{Z}(C)|$. Due to conjugacy, we can integrate out the model parameters θ_γ from the posterior distribution $p(C, \theta_\gamma|\boldsymbol{\Xi})$ and estimate solely the posterior of the latent variable C, $p(C|\boldsymbol{\Xi}, \boldsymbol{\Delta}, \alpha, \lambda) = \frac{p(C \mid \boldsymbol{\Delta},\alpha)p(\boldsymbol{\Xi}|\mathbf{Z}(C),\lambda)}{\sum_C p(C \mid \boldsymbol{\Delta},\alpha)p(\boldsymbol{\Xi}|\mathbf{Z}(C),\lambda)}$. As this full posterior is intractable, we approximate it via Collapsed Gibbs sampling, by drawing samples of c_i from the following posterior distribution,

$$\begin{aligned} c_i &\sim \dot{\boldsymbol{\xi}}\text{-}\mathcal{SD}\text{-}\mathcal{CRP}(\boldsymbol{\Delta}, \alpha) \\ z_i &= \mathbf{Z}(c_i) \\ \theta_\gamma^k &\sim \mathcal{NIW}(\lambda_0) \\ \boldsymbol{\xi}_i | z_i = k &\sim \mathcal{N}(\theta_\gamma^k) \end{aligned} \tag{6}$$

$$p(c_i = j \mid C_{-i}, \boldsymbol{\Xi}, \boldsymbol{\Delta}, \alpha, \lambda) \;\propto\; \underbrace{p(c_i = j \mid \boldsymbol{\Delta}, \alpha)}_{\substack{\text{Similarities in} \\ \text{Scaled-Velocity Space}}} \underbrace{p(\boldsymbol{\Xi} \mid \mathbf{Z}(c_i = j \cup C_{-i}), \lambda)}_{\substack{\text{Observations in} \\ \text{Position Space}}} \tag{7}$$

where the first term is given by (5) and the second term is the likelihood of the table assignments that emerge from the current seating arrangement $\mathbf{Z}(c_i = j \cup C_{-i})$. C_{-i} indicates the customer seating assignments for all customers except the i-th. Due to conjugacy with the $\mathcal{NIW}$, the likelihood term has an analytical solution, see Appendix D.1 in the Supplementary Material. (7) holds some particularities as opposed to the standard collapsed conditionals and mixture models. First, the prior is represented through the latent variables C, while the likelihood is in terms of Z. Furthermore, the key component behind what makes this mixture *physically-consistent* is the fact that the prior uses

similarity measures from the scaled-velocity space, while the likelihood is computed solely on the observations which live in the Euclidean-position space. In terms of computation, the likelihood is computed for all points $\boldsymbol{\Xi}$, rather than just for the sampled point $\boldsymbol{\xi}_i$, this is due to the fact that the partition of the dataset depends on C and not on Z. A new sample c_i affects the overall partition; e.g. a table could be split or two tables could be merged; all because the customers are not conditionally independent of the other customers' assignments. Hence, this effect must be taken into consideration after each iteration in the sampler. We adapt the Collapsed Gibbs sampler proposed by [21] and apply it to our mixture model setting. Details are reported in Appendix D.3.

2.4 Estimating the GMM parameters θ_γ from table assignments $\mathbf{Z}(C)$ and $\mathcal{NIW}$

After running the sampler on (7) for a pre-defined number of T iterations, the iteration with the $\max \log$ posterior conditional probability is chosen as the optimal partition; i.e. the MAP (Maximum A Posteriori) estimate. This gives us the MAP estimate of the optimal number of Gaussians $K = |\mathbf{Z}(C)|$ and the observations that are assigned to each Gaussian $\boldsymbol{\Xi}_{\mathbf{Z}(C)=k}$. Hence, to estimate the table parameters (i.e. Gaussian parameters) $\{\boldsymbol{\mu}^k, \boldsymbol{\Sigma}^k\}_{k=1}^K$ we take $\boldsymbol{\Xi}_{\mathbf{Z}(C)=k}$ for each k-th cluster and the set of hyper-parameters λ and sample the Gaussian parameters $\boldsymbol{\mu}^k, \boldsymbol{\Sigma}^k$ from the posterior of the $\mathcal{NIW}$, refer to Appendix D.2 for exact equations. Finally, the mixing weights $\{\pi_k\}_{k=1}^K$ are estimated as $\pi_k = M_k/M$, where $M_k = |\boldsymbol{\Xi}_{\mathbf{Z}(C)=k}|$ is the number of observations assigned to the k-th cluster. In Figure 1 we show the performance of our $\mathcal{PC}$-GMM vs. a $\mathcal{CRP}$-GMM estimated via Collaped Gibbs Sampling and the finite GMM estimated via EM on two challenging datasets, on an exemplary dataset of the *concentric* circular trajectories. Further exemplars of challenging datasets in which $\mathcal{PC}$-GMM outperforms all approaches are provided in Appendix E[1].

3 Physically Consistent GMM-based LPV-DS Learning

To model non-linear motions from demonstrations, we parametrize the mixture of linear DS (1) in a decoupled manner [18]. Given the set of reference trajectories $\{\boldsymbol{\Xi}, \dot{\boldsymbol{\Xi}}\} = \{\boldsymbol{\xi}_{\boldsymbol{t}}^{\text{ref}}, \dot{\boldsymbol{\xi}}_{\boldsymbol{t}}^{\text{ref}}\}_{t=1\dots T_N}$ and the attractor $\boldsymbol{\xi}^*$ (i.e. the desired target), we begin by learning the GMM parameters $\theta_\gamma = \{\pi_k, \boldsymbol{\mu}^k, \boldsymbol{\Sigma}^k\}_{k=1}^K$ via the approach presented in Section 2. Then, we estimate the parameters for the individual DS $\theta_f = \{\mathbf{A}_k, \boldsymbol{b}_k\}_{k=1}^K$ by minimizing the velocity error between the approximated desired velocity given by (1) and the observed velocity from the reference trajectories $\dot{\boldsymbol{\xi}}^{\text{ref}}$. This can be formulated as minimizing the following objective function:

$$\min_{\theta_f} J(\theta_f) = \sum_{n=1}^{N_{\text{ref}}} \sum_{t=1}^{T_N} ||\dot{\boldsymbol{\xi}}_{\boldsymbol{t},\boldsymbol{m}}^{\text{ref}} - \mathbf{f}(\boldsymbol{\xi}_{\boldsymbol{t},\boldsymbol{m}}^{\text{ref}})||^2 \tag{8}$$

where N_{ref} is the number of reference trajectories, T_N is the number of samples in each trajectory and $\mathbf{f}(\cdot)$ is given by (1). Depending on the *sufficient stability conditions* for the system parameters $\mathbf{A}_k, \boldsymbol{b}_k$, different constrained optimization problems can be formulated.

3.1 Generalized GMM-based LPV-DS Learning

Due to the decoupling of the parameters in the LPV-DS formulation, imposing constraints on the DS parameters is quite flexible. Following, we propose 3 constraint variants to solve (8) derived from: (O1) a QLF (like SEDS) [8], (O2) a conservative P-QLF as in [18] and (O3) a less conservative P-QLF (following the proposition in Appendix B):

$$\begin{aligned}
&\min_{\theta} J(\theta) \quad \text{subject to} \\
&(O1) \left\{ (\mathbf{A}_k)^T + \mathbf{A}_k \prec 0, \boldsymbol{b}_k = -\mathbf{A}_k \boldsymbol{\xi}^* \ \ \forall k = 1, \dots, K \right. \\
&(O2) \left\{ (\mathbf{A}_k)^T \mathbf{P} + \mathbf{P}\mathbf{A}_k \prec 0, \ \ \boldsymbol{b}_k = \vec{0} \ \ \forall k = 1, \dots, K; \ \ \mathbf{P} = \mathbf{P}^T \succ 0 \right. \\
&(O3) \left\{ (\mathbf{A}_k)^T \mathbf{P} + \mathbf{P}\mathbf{A}_k \prec \mathbf{Q}_k, \ \ \mathbf{Q}_k = \mathbf{Q}_k^T \prec 0, \ \ \boldsymbol{b}_k = -\mathbf{A}_k \boldsymbol{\xi}^* \ \ \forall k = 1, \dots, K \right.
\end{aligned} \tag{9}$$

$(O1)$ follows the same conditions used in SEDS, yet, instead of it being a non-linear constrained optimization problem, it is a convex semidefinite optimization problem which can be solved via standard semi-definite programming solvers such as SeDuMi [23]. This approach is comparable to SEDS and will be exploited for our incremental learning approach in Section 5. $(O2)$ has non-convex constraints as $\mathbf{P}$ is unknown, yet it can be solved via non-linear semi-definite programming

[1] MATLAB code for $\mathcal{PC}$-GMM+datasets available at: https://github.com/nbfigueroa/phys-gmm

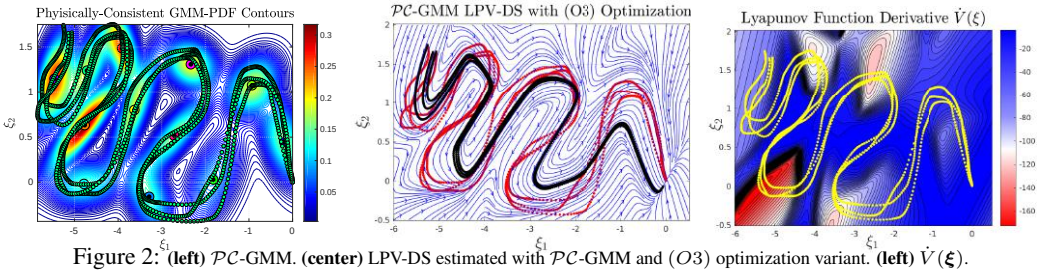

Figure 2: **(left)** $\mathcal{PC}$-GMM. **(center)** LPV-DS estimated with $\mathcal{PC}$-GMM and $(O3)$ optimization variant. **(left)** $\dot{V}(\boldsymbol{\xi})$.

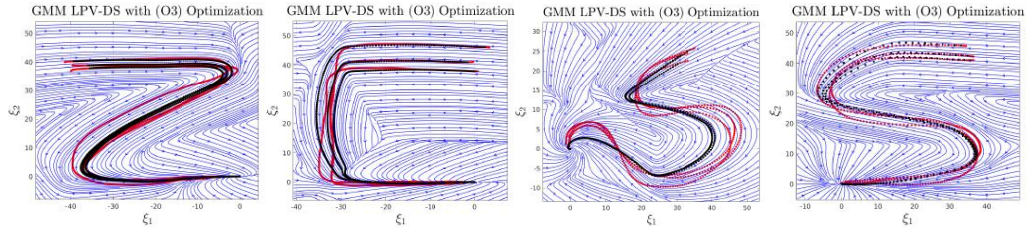

Figure 3: GMM-based LPV-DS estimated via $(O3)$ on exemplary models learned from the LASA handwriting dataset.

solvers, such as PENLAB [24]. Note that $(O2)$ assumes the attractor is at the origin, hence the constraint $\boldsymbol{b}_k = \vec{0}$, without this assumption it may converge to unstable solutions. We propose $(O3)$, where we assume to have a prior estimate of $\mathbf{P}$ obtained through the data-driven approach presented in [25], which learns a weighted sum of asymmetric quadratic functions (WSAQF) from data. Yet, we simplify the optimization problem by allowing only one P-QLF. Given such prior estimate of $\mathbf{P}$, we introduce the auxiliary matrices $\mathbf{Q}_k$ which allow for a wider exploration of the parameter space. $(O3)$ is also a non-convex semidefinite program, which we solve with PENLAB. In this work we use the aformentioned solver with the YALMIP MATLAB toolbox [26]. $(O2)$ yields similar results as $(O3)$ when it finds a feasible solution. Due to the non-linearity of the problem it might converge to a solution where not all of the constraints are met. $(O3)$ always converges to a feasible solution, as long as $\mathbf{P} = \mathbf{P}^T$ and has well-balance eigenvalues. In Figure 2 and 3 we show the results of $(O3)$ on the *messy-snake* trajectories and *four motions* from the LASA dataset, respectively. The latter motions are known to be challenging for QLF-based methods. While the *messy-snake* dataset is even more challenging, our method is capable of approximating the highly-curved motion. For further $(O\cdot)$-comparisons see Appendix G[2].

4 Evaluation and Experiments

Learning Evaluation We quantitatively evaluate the *physical consistency* of our proposed methodology on the entire LASA dataset (excluding the multi-model motions); i.e. 26 handwritten motion sets. Each motion set contains 7 trajectories, 4 are used to *train* our models and evaluate *reproduction accuracy* and the remaining 3 are used to *test* generalization accuracy; i.e. reproduction accuracy of unseen trajectories. We employ three metrics: (i) prediction RMSE $= \frac{1}{M}\sum_{m=1}^{M} ||\dot{\boldsymbol{\xi}}_{\boldsymbol{m}}^{\text{ref}} - \mathbf{f}(\boldsymbol{\xi}_{\boldsymbol{m}}^{\text{ref}})||$ as in [11], (ii) prediction cosine similarity $\dot{e} = \frac{1}{M}\sum_{m=1}^{M}\left|1 - \frac{\mathbf{f}(\boldsymbol{\xi}_{\boldsymbol{m}}^{\text{ref}})^T \dot{\boldsymbol{\xi}}_{\boldsymbol{m}}^{\text{ref}}}{||\mathbf{f}(\boldsymbol{\xi}_{\boldsymbol{m}}^{\text{ref}})||||\dot{\boldsymbol{\xi}}_{\boldsymbol{m}}^{\text{ref}}||}\right|$ as in [18] and (iii) dynamic time warping distance (DTWD) as in [13]. While (i-ii) give an overall similarity of the shape of the resulting DS wrt. the demonstrations, (iii) measures the dissimilarity between the shapes of the reference trajectories and their corresponding reproductions from the same initial points. Figure 4 shows the performance of SEDS (S), EM-based GMM $E(\cdot)$ fitting and $\mathcal{PC}$-GMM $PC(\cdot)$ with $(O1-3)$ LPV-DS optimization variants from (9). RMSE is comparable throughout all methods as this metric is not representative of reproduction accuracy. If we focus on $\dot{e}$ and the DTWD on the *training* set, methods $E(O2-3)$ and $PC(O2-3)$ clearly outperform SEDS with a drastic gap in the DTWD. This is due to motions as the ones illustrated in Figure 3 where SEDS either diverges or goes directly to the attractor. While the $E(O2-3)$ approaches have comparable accuracy on the *training* set, their error increase on the *testing* set. This indicates that the $E(O2-3)$ are over-fitting and only locally shaping the DS, yet the overall shape of the motion is not being generalized. The relative train/test errors for our approach, on the other, tend to be in the same range. Further evidence of this behavior on 11 challenging motions from the LASA dataset is provided in Appendix G.

[2]MATLAB code for DS-optimization+datasets available at: `https://github.com/nbfigueroa/ds-opt`

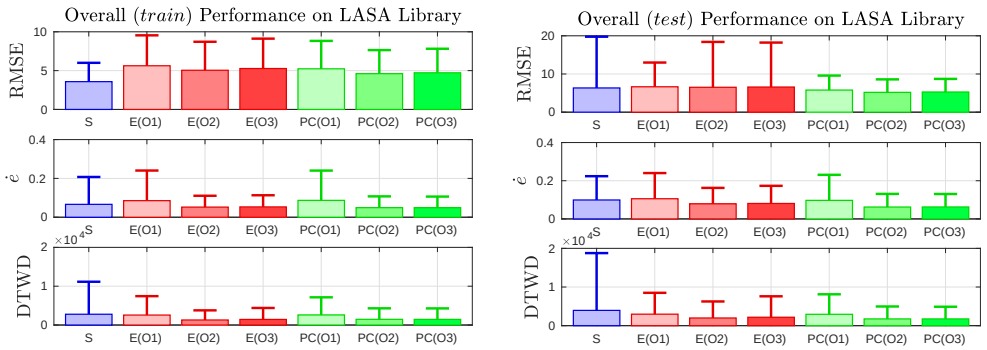

Figure 4: Overall Performance Metrics on LASA Library. **(Left)** Performance on the *training* data. **(Right)** Performance on the *testing* data. Each bar-graph shows the mean (and std.) of the error for every approach. S=SEDS, $E(\cdot)$=EM-GMM, $PC(\cdot)$=PC-GMM and $(O1-3)$ stands for the type of optimization variants.

Robotic Experiments The proposed approach was used to learn complex motions for three real-world scenarios involving: (i) an inspection-line task, (ii) a branding-line task and (iii) a shelf-arranging task, as depicted in Figure 5 for task (i). Videos of the learning and execution of these tasks are provided in the following link: `http://lasa.epfl.ch/files/Nadia/Figueroa-CoRL2018-Experiments.mp4`

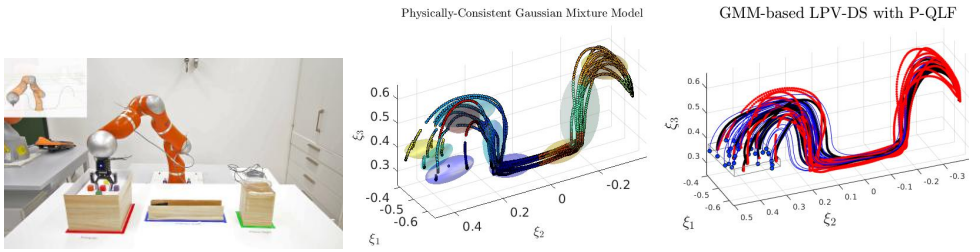

Figure 5: *Inspection* task. **(center)** $\mathcal{PC}$-GMM. **(right)** LPV-DS estimated with $\mathcal{PC}$-GMM and $(O3)$ optimization variant.

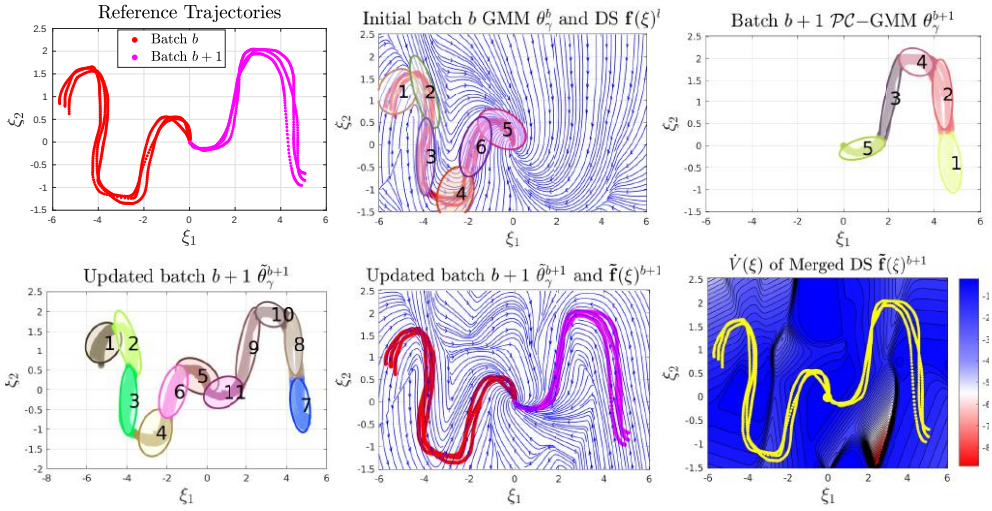

Figure 6: Illustration of Incremental $\mathcal{PC}$-GMM-based LPV-DS Learning Approach.

5 Towards Incremental Learning of LPV Dynamical Systems

Problem Setting: Assume we obtained an initial batch, $b=1$, of reference trajectories $\{\boldsymbol{\Xi}, \dot{\boldsymbol{\Xi}}\}^b = \{\boldsymbol{\xi}_t^{\text{ref}}, \dot{\boldsymbol{\xi}}_t^{\text{ref}}\}_{t=1\ldots T_N}^b$ we then learn a DS $\mathbf{f}^b(\boldsymbol{\xi})$ on these demonstrations and use it to generate motions. After a while, we obtain a new batch of reference trajectories $\{\boldsymbol{\Xi}, \dot{\boldsymbol{\Xi}}\}^{b+1}$ that we wish to use to update the DS $\mathbf{f}^b(\boldsymbol{\xi}) \rightarrow \tilde{\mathbf{f}}^{b+1}(\boldsymbol{\xi})$, and so on. A naive approach to tackle this problem would be to simply concatenate the batches of reference trajectories $\{\boldsymbol{\Xi}, \dot{\boldsymbol{\Xi}}\} = \{\boldsymbol{\Xi}, \dot{\boldsymbol{\Xi}}\}^b \cup \{\boldsymbol{\Xi}, \dot{\boldsymbol{\Xi}}\}^{b+1} \cup \cdots \cup$

$\{\Xi, \dot{\Xi}\}^{b+\infty}$ and learn a new DS every time new data arrives. Such an approach becomes not only computationally expensive as the number of batches increases, and is *data-inefficient* as it does not use the previous batches of data in an efficient way. For example, if a new reference trajectory arrives, that is overlapping with trajectories from the old batches, learning new parameters θ_γ and θ_f might have no effect on the resulting model, hence there is no need to re-learn the DS. Another example of such *data-inefficiency* occurs if the batches of reference trajectories are non-overlapping as in the example in Figure 6, it is not necessary to learn the DS parameters θ_f^b associated to the previous batch from scratch. In lieu if these observations, we propose an incremental learning algorithm that can *update* a DS $\mathbf{f}^b(\boldsymbol{\xi})$ learned on a dataset $\{\Xi, \dot{\Xi}\}^b$ with new incoming reference trajectories $\{\Xi, \dot{\Xi}\}^{b+1}$, while (i) re-using the parameters θ_γ^b and θ_f^b learned from the previous batch, (ii) solely using the newly arrived batch of data $\{\Xi, \dot{\Xi}\}^{b+1}$ and (iii) preserving *GAS*.

An Incremental Learning Approach for LPV-DS Consider each batch of demonstrations $\{\Xi, \dot{\Xi}\}^b$ and $\{\Xi, \dot{\Xi}\}^{b+1}$ representing two independent DS,

$$\mathbf{f}^b(\boldsymbol{\xi}) = \sum_{k=1}^{K^b} \gamma_k^b(\boldsymbol{\xi})(\mathbf{A}_k^b\boldsymbol{\xi} + \boldsymbol{b}_k^b), \;\; \mathbf{f}^{b+1}(\boldsymbol{\xi}) = \sum_{k=1}^{K^{b+1}} \gamma_k^{b+1}(\boldsymbol{\xi})\Big(\mathbf{A}_k^{b+1}\boldsymbol{\xi} + \boldsymbol{b}_k^{b+1}\Big) \tag{10, 11}$$

The updated DS $\tilde{\mathbf{f}}^{b+1}(\boldsymbol{\xi}) = \mathbf{f}^b(\boldsymbol{\xi}) \oplus \mathbf{f}^{b+1}(\boldsymbol{\xi})$ is constructed by merging (10) and (11), with operator $\oplus$ denoting the merge operation of two functions. In order for $\tilde{\mathbf{f}}^{b+1}(\boldsymbol{\xi})$ to be globally asymptotically stable we propose the following sufficient conditions which are derived from a QLF:

Theorem 1 *The merged DS $\tilde{\mathbf{f}}^{b+1}(\boldsymbol{\xi}) = \mathbf{f}^b(\boldsymbol{\xi}) \oplus \mathbf{f}^{b+1}(\boldsymbol{\xi})$ composed of individual DS (10) and (11) is globally asymptotically converging at the attractor $\boldsymbol{\xi}^*$ iff,*

$$\begin{aligned}
&\sum_{k=1}^{K^b} \gamma_k^b(\boldsymbol{\xi}) + \sum_{k=1}^{K^{b+1}} \gamma_k^{b+1}(\boldsymbol{\xi}) = 1 \\
&(\mathbf{A}_k^b)^T + \mathbf{A}_k^b \prec 0, \;\; \boldsymbol{b}_k^b = -\mathbf{A}_k\boldsymbol{\xi}^* \qquad\qquad \forall\, k = 1, \dots, K^b \\
&(\mathbf{A}_k^{b+1})^T + \mathbf{A}_k^{b+1} \prec 0, \;\; \boldsymbol{b}_k^{b+1} = -\mathbf{A}_k\boldsymbol{\xi}^* \quad \forall\, k = 1, \dots, K^{b+1}
\end{aligned} \tag{12}$$

Proof: *See Appendix F.* ■

Updating the mixing function $\theta_\gamma^b \rightarrow \theta_\gamma^{b+1}$ from new data Given new data $\theta_\gamma^b \rightarrow \theta_\gamma^{b+1}$ we learn a new $\mathcal{PC}$-GMM θ_γ^{b+1}. We then follow the incremental estimation of GMMs approach for online data stream clustering approach presented in [27]. However, instead of using multivariate statistical tests for equality of covariance and mean as a merging strategy, we use the Kullback-Leibler Divergence $D_{KL}(\mathcal{N}(\boldsymbol{\mu}_k^b, \boldsymbol{\Sigma}_k^b)||\mathcal{N}(\boldsymbol{\mu}_k^{b+1}, \boldsymbol{\Sigma}_k^{b+1}))$ between each k-th Gaussian component of each GMM. If any biderectional $D_K L < \tau$ is less than a threshold τ, normally set to 1, then the Gaussians are deemed similar and their sufficient statistics are used to update the components. Illustrative results of this procedure are shown in Figures 16 and Figure 6 for examples that need and don't need merging of Gaussians.

Compute DS parameters $\theta_f^b \rightarrow \theta_f^{b+1}$ for new local components For the new set of Gaussian components created from the previous step we now compute the DS parameters θ_γ^{b+1} on the newly arrived training data $\{\Xi, \dot{\Xi}\}^{b+1}$ by solving the convex optimization problem (9) with variant $(O1)$.

6 Discussion and Future Work

The main contribution of this work is the $\mathcal{PC}$-GMM that is capable of fitting GMM to trajectory data in a physically consistent way. This enabled us to provide accurate estimations of LPV-DS that outperform SEDS and further propose an incremental learning strategy for LPV-DS that preserves global asymptotic stability. One drawback of our approach is the computational complexity of the Collapsed Gibbs Sampler. As highlighted in [21] at each iteration all points are visited, hence, making the initial iterations computationally heavy if many points are used. Our future directions involve optimizing such computations and extending the incremental algorithm such that it can employ the P-QLF in order to model more complex motions as the offline generalized LPV-DS approach proposed in Section 3.

Acknowledgments

This work was supported by the EU project Cogimon H2020-ICT-23-2014.

References

[1] D. Kulic, D. Kragic, and V. Krüger. Learning action primitives. In *Visual Analysis of Humans*, pages 333–353. Springer, 2011. ISBN 978-0-85729-996-3.

[2] A. Billard, S. Calinon, R. Dillmann, and S. Schaal. Robot programming by demonstration. In *Springer Handbook of Robotics*, pages 1371–1394. 2008.

[3] B. Argall, S. Chernova, M. Veloso, and B. Browning. A survey of robot learning from demonstration. *Robotics and Autonomous Systems*, 57(5):469–483, 2009.

[4] S. Schaal, C. Atkeson, and S. Vijayakumar. Scalable techniques from nonparametric statistics for real time robot learning. *Applied Intelligence*, 17(1):49–60, 2002.

[5] A. Shon, K. Grochow, and R. Rao. Robotic imitation from human motion capture using gaussian processes. In *Humanoids*, pages 129–134. IEEE, 2005. ISBN 0-7803-9320-1.

[6] S. Calinon, F. Guenter, and A. Billard. On learning, representing, and generalizing a task in a humanoid robot. *IEEE Transactions on SMC, Part B*, 37(2):286–298, 2007.

[7] E. Gribovskaya, S. M. Khansari Zadeh, and A. Billard. Learning Nonlinear Multivariate Dynamics of Motion in Robotic Manipulators. *International Journal of Robotics Research*, 2010. ISSN 0278-3649. doi:NA.

[8] S. Khansari-Zadeh and A. Billard. Learning stable nonlinear dynamical systems with gaussian mixture models. *Robotics, IEEE Transactions on*, 27(5):943–957, Oct 2011.

[9] S. M. Khansari-Zadeh and A. Billard. Learning control lyapunov function to ensure stability of dynamical system-based robot reaching motions. *Robotics and Autonomous Systems*, 62(6): 752 – 765, 2014. ISSN 0921-8890.

[10] S. S. M. Salehian, M. Khoramshahi, and A. Billard. A dynamical system approach for softly catching a flying object: Theory and experiment. *IEEE Transactions on Robotics*, 32(2):462–471, April 2016.

[11] J. R. Medina and A. Billard. Learning stable task sequences from demonstration with linear parameter varying systems and hidden markov models. In *1st Annual Conference on Robot Learning, CoRL 2017, Mountain View, California, USA, November 13-15, 2017, Proceedings*, pages 175–184, 2017.

[12] K. Neumann and J. J. Steil. Learning robot motions with stable dynamical systems under diffeomorphic transformations. *Robotics and Autonomous Systems*, 70(Supplement C):1 – 15, 2015. ISSN 0921-8890.

[13] H. Ravichandar, I. Salehi, and A. Dani. Learning partially contracting dynamical systems from demonstrations. In S. Levine, V. Vanhoucke, and K. Goldberg, editors, *Proceedings of the 1st Annual Conference on Robot Learning*, volume 78 of *Proceedings of Machine Learning Research*, pages 369–378. PMLR, 13–15 Nov 2017.

[14] A. Lemme, K. Neumann, R. Reinhart, and J. Steil. Neural learning of vector fields for encoding stable dynamical systems. *Neurocomputing*, 141(0):3 – 14, 2014. ISSN 0925-2312.

[15] C. Blocher, M. Saveriano, and D. Lee. Learning stable dynamical systems using contraction theory. In *2017 14th International Conference on Ubiquitous Robots and Ambient Intelligence (URAI)*, pages 124–129, June 2017. doi:10.1109/URAI.2017.7992901.

[16] N. Perrin and P. Schlehuber-Caissier. Fast diffeomorphic matching to learn globally asymptotically stable nonlinear dynamical systems. *Systems & Control Letters*, 96(Supplement C):51 – 59, 2016. ISSN 0167-6911.

[17] P. Apkarian, P. Gahinet, and G. Becker. Self-scheduled h∞ control of linear parameter-varying systems: a design example. *Automatica*, 31(9):1251 – 1261, 1995.

[18] S. S. Mirrazavi Salehian. Compliant control of uni/multi- robotic arms with dynamical systems. Phd Thesis, IMT, EPFL, 2018.

[19] Y. Shavit, N. Figueroa, S. S. Mirrazavi Salehian, and A. Billard. Learning augmented joint-space task-oriented dynamical systems: A linear parameter varying and synergetic control approach. IEEE Robotics and Automation Letters (RA-L), 2018.

[20] R. Jonschkowski, S. Höfer, and O. Brock. Patterns for Learning with Side Information. *ArXiv e-prints*, Nov. 2015.

[21] D. M. Blei and P. I. Frazier. Distance dependent chinese restaurant processes. *J. Mach. Learn. Res.*, 12:2461–2488, Nov. 2011.

[22] M. I. Jordan. Dirichlet processes, chinese restaurant processes and all that. In *NIPS 2005*, 2005.

[23] J. F. Sturm. Using sedumi 1.02, a matlab toolbox for optimization over symmetric cones. *Optimization Methods and Software*, 11(1-4):625–653, 1999.

[24] J. Fiala, M. Kočvara, and M. Stingl. PENLAB: A MATLAB solver for nonlinear semidefinite optimization. *ArXiv e-prints*, Nov. 2013.

[25] S. M. Khansari-Zadeh and O. Khatib. Learning potential functions from human demonstrations with encapsulated dynamic and compliant behaviors. *Autonomous Robots*, pages 1–25, 2015. ISSN 1573-7527.

[26] J. Lofberg. Yalmip : a toolbox for modeling and optimization in matlab. In *2004 IEEE International Conference on Robotics and Automation (IEEE Cat. No.04CH37508)*, pages 284–289, Sept 2004. doi:10.1109/CACSD.2004.1393890.

[27] M. Song and H. Wang. Highly efficient incremental estimation of Gaussian mixture models for online data stream clustering. In K. L. Priddy, editor, *Society of Photo-Optical Instrumentation Engineers (SPIE) Conference Series*, volume 5803 of *Presented at the Society of Photo-Optical Instrumentation Engineers (SPIE) Conference*, pages 174–183, March 2005. doi:10.1117/12.601724.

[28] A. Gelman, J. B. Carlin, H. S. Stern, and D. B. Rubin. *Bayesian Data Analysis*. Chapman and Hall/CRC, 2003.

[29] K. P. Murphy. Conjugate bayesian analysis of the gaussian distribution. Technical report, 2007.

Appendix

A Stability of a Linear DS with Parametrized QLF

We wish to prove the following proposition:

Proposition 1 *A linear DS of the form $\dot{\boldsymbol{\xi}} = \mathbf{A}\boldsymbol{\xi} + \boldsymbol{b}$ is globally asymptotically converging at the attractor $\boldsymbol{\xi}^*$ iff,*

$$\begin{cases} \mathbf{A}^T\mathbf{P} + \mathbf{P}\mathbf{A} \prec \mathbf{Q}, \;\; \mathbf{P} \succ 0, \qquad \mathbf{Q} \prec 0 \\ \boldsymbol{b} = -\mathbf{A}\boldsymbol{\xi}^* \end{cases} \tag{13}$$

where $\prec$ (and $\succ$) refer to negative (and positive) definiteness of a matrix, respectively. Recall that a matrix $\mathbf{A}$ is deemed negative (or positive) definite iff it's symmetric part $\tilde{\mathbf{A}} = \frac{1}{2}(\mathbf{A}^T + \mathbf{A})$ has all negative (or positive) eigenvalues. Both $\mathbf{P} \in \mathbb{R}^{M\times M}$ and $\mathbf{Q} \in \mathbb{R}^{M\times M}$ are symmetric.

Proof: This can be proven if there exists a continuous and continuously differentiable Lyapunov function $V(\boldsymbol{\xi}) : \mathbb{R}^N \to \mathbb{R}$ such that $V(\boldsymbol{\xi}) \succ 0, \dot{V}(\boldsymbol{\xi}) \prec 0 \; \forall \, \boldsymbol{\xi} \neq \boldsymbol{\xi}^*$ and $V(\boldsymbol{\xi}^*) = 0, \dot{V}(\boldsymbol{\xi}^*) = 0$. By considering the P-QLF candidate function of the following form:

$$V(\boldsymbol{\xi}) = (\boldsymbol{\xi} - \boldsymbol{\xi}^*)^T\mathbf{P}(\boldsymbol{\xi} - \boldsymbol{\xi}^*) \tag{14}$$

we can ensure $V(\boldsymbol{\xi}) > 0$ due to its quadratic form. The second condition follows by taking the derivative of $V(\boldsymbol{\xi})$ wrt. time, given a symmetric $\mathbf{P}$,

$$\begin{aligned} \dot{V}(\boldsymbol{\xi}) &= (\boldsymbol{\xi} - \boldsymbol{\xi}^*)^T\mathbf{P}\mathbf{f}(\boldsymbol{\xi}) + \mathbf{f}(\boldsymbol{\xi})^T\mathbf{P}(\boldsymbol{\xi} - \boldsymbol{\xi}^*) \\ &= (\boldsymbol{\xi} - \boldsymbol{\xi}^*)^T\mathbf{P}\underbrace{(\mathbf{A}\boldsymbol{\xi} + \boldsymbol{b})}_{\text{via (13)}} + \underbrace{(\mathbf{A}\boldsymbol{\xi} + \boldsymbol{b})^T}_{\text{via (13)}}\mathbf{P}(\boldsymbol{\xi} - \boldsymbol{\xi}^*) \\ &= (\boldsymbol{\xi} - \boldsymbol{\xi}^*)^T\mathbf{P}(\mathbf{A}\boldsymbol{\xi} - \underbrace{\mathbf{A}\boldsymbol{\xi}^*}_{\text{via (13)}}) + (\mathbf{A}\boldsymbol{\xi} - \underbrace{\mathbf{A}\boldsymbol{\xi}^*}_{\text{via (13)}})^T\mathbf{P}(\boldsymbol{\xi} - \boldsymbol{\xi}^*) \\ &= (\boldsymbol{\xi} - \boldsymbol{\xi}^*)^T\mathbf{P}\mathbf{A}(\boldsymbol{\xi} - \boldsymbol{\xi}^*) + (\boldsymbol{\xi} - \boldsymbol{\xi}^*)^T\mathbf{A}^T\mathbf{P}(\boldsymbol{\xi} - \boldsymbol{\xi}^*) \\ &= (\boldsymbol{\xi} - \boldsymbol{\xi}^*)^T\Big[\underbrace{\mathbf{P}\mathbf{A} + \mathbf{A}^T\mathbf{P}}_{\mathbf{Q}\prec 0 \;\; \text{via} \;\; (13)}\Big](\boldsymbol{\xi} - \boldsymbol{\xi}^*) < 0 \end{aligned} \tag{15}$$

with $\mathbf{Q} = \mathbf{Q}^T \prec 0$. By substituting $\boldsymbol{\xi} = \boldsymbol{\xi}^*$ in (14) and (15) we ensure $V(\boldsymbol{\xi}^*) = 0, \dot{V}(\boldsymbol{\xi}^*) = 0$. Therefore, the linear DS is *globally asymptotically stable* with respect to an attractor $\boldsymbol{\xi}^*$ if conditions (13) are satisfied. ■

B Stability of a Non-Linear DS with Parametrized QLF

We wish to prove the following proposition:

Proposition 2 *The nonlinear DS defined in* (1) *is globally asymptotically converging at the attractor $\boldsymbol{\xi}^*$ iff,*

$$(\mathbf{A}_k)^T\mathbf{P} + \mathbf{P}\mathbf{A}_k \prec \mathbf{Q}_k, \;\; \mathbf{Q}_k = \mathbf{Q}_k^T \prec 0, \;\; \boldsymbol{b}_k = -\mathbf{A}_k\boldsymbol{\xi}^* \;\; \forall k = 1, \ldots, K \tag{16}$$

Proof: This can be proven if there exists a continuous and continuously differentiable Lyapunov function $V(\boldsymbol{\xi}) : \mathbb{R}^N \to \mathbb{R}$ such that $V(\boldsymbol{\xi}) \succ 0, \dot{V}(\boldsymbol{\xi}) \prec 0 \; \forall \, \boldsymbol{\xi} \neq \boldsymbol{\xi}^*$ and $V(\boldsymbol{\xi}^*) = 0, \dot{V}(\boldsymbol{\xi}^*) = 0$. By considering a parametrized quadratic Lyapunov candidate function as in (14), we can ensure $V(\boldsymbol{\xi}) > 0$ due to its quadratic form. The second condition follows by taking the derivative of $V(\boldsymbol{\xi})$

wrt. time, given a symmetric $\mathbf{P}$,

$$
\begin{aligned}
\dot{V}(\boldsymbol{\xi}) &= (\boldsymbol{\xi}-\boldsymbol{\xi}^*)^T\mathbf{P}\mathbf{f}(\boldsymbol{\xi}) + \mathbf{f}(\boldsymbol{\xi})^T\mathbf{P}(\boldsymbol{\xi}-\boldsymbol{\xi}^*) \\
&= (\boldsymbol{\xi}-\boldsymbol{\xi}^*)^T\mathbf{P}\underbrace{\Big(\sum_{k=1}^{K}\gamma_k(\boldsymbol{\xi})(\mathbf{A}_k\boldsymbol{\xi}+\boldsymbol{b}_k)\Big)}_{\text{via (16)}} + \underbrace{\Big(\sum_{k=1}^{K}\gamma_k(\boldsymbol{\xi})(\mathbf{A}_k\boldsymbol{\xi}+\boldsymbol{b}_k)^T\Big)}_{\text{via (16)}}\mathbf{P}(\boldsymbol{\xi}-\boldsymbol{\xi}^*) \\
&= (\boldsymbol{\xi}-\boldsymbol{\xi}^*)^T\mathbf{P}\Big(\sum_{k=1}^{K}\gamma_k(\boldsymbol{\xi})(\mathbf{A}_k\boldsymbol{\xi}-\underbrace{\mathbf{A}\boldsymbol{\xi}^*}_{\text{via (16)}})\Big) + \Big(\sum_{k=1}^{K}\gamma_k(\boldsymbol{\xi})(\mathbf{A}_k\boldsymbol{\xi}-\underbrace{\mathbf{A}\boldsymbol{\xi}^*}_{\text{via (16)}})^T\Big)\mathbf{P}(\boldsymbol{\xi}-\boldsymbol{\xi}^*) \\
&= (\boldsymbol{\xi}-\boldsymbol{\xi}_g^*)^T\mathbf{P}_g\Big(\sum_{k=1}^{K}\gamma_k(\boldsymbol{\xi})\mathbf{A}_k\Big)(\boldsymbol{\xi}-\boldsymbol{\xi}^*) \quad + (\boldsymbol{\xi}-\boldsymbol{\xi}^*)^T\Big(\sum_{k=1}^{K}\gamma_k(\boldsymbol{\xi})(\mathbf{A}_k)^T\Big)\mathbf{P}(\boldsymbol{\xi}-\boldsymbol{\xi}^*) \\
&= (\boldsymbol{\xi}-\boldsymbol{\xi}^*)^T\Big(\sum_{k=1}^{K}\underbrace{\gamma_k(\boldsymbol{\xi})}_{>0 \text{ via (1)}}\underbrace{(\mathbf{P}\mathbf{A}_k+(\mathbf{A}_k)^T\mathbf{P})}_{\prec\mathbf{Q}_k \text{ via (16)}}\Big)(\boldsymbol{\xi}-\boldsymbol{\xi}^*) < 0
\end{aligned}
\tag{17}
$$

with $\mathbf{Q}_k = \mathbf{Q}_k^T \prec 0$. By substituting $\boldsymbol{\xi} = \boldsymbol{\xi}^*$ in (14) and (17) we ensure $V(\boldsymbol{\xi}^*) = 0, \dot{V}(\boldsymbol{\xi}^*) = 0$. Therefore, (1) is globally asymptotically stable with respect to an attractor $\boldsymbol{\xi}^*$ if conditions (16) are satisfied. □

C Graphical Model of Physically Consistent Bayesian Non-Parametric Gaussian Mixture Model

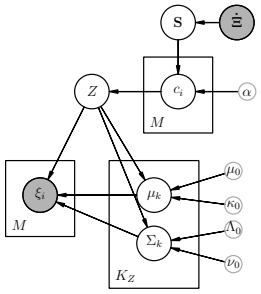

Figure 7: Graph. model of $\mathcal{PC}$-GMM.

D Collapsed Gibbs Sampler and Sampling Equations for Section 2

D.1 Likelihood of Partitions for $Z = \mathbf{Z}(C)$

The likelihood of a partition $Z = \mathbf{Z}(C)$ is computed as the product of the probabilities of the customers $\boldsymbol{\Xi}$ sitting at their assigned tables Z,

$$
p(\boldsymbol{\Xi}|\mathbf{Z}(C),\lambda) = \prod_{k=1}^{|\mathbf{Z}(C)|} p(\boldsymbol{\Xi}_{\mathbf{Z}(C)=k}|\lambda) \tag{18}
$$

where $|\mathbf{Z}(C)|$ denotes the number of unique tables emerged from $\mathbf{Z}(C)$; i.e. K in a finite mixture model, and $\mathbf{Z}(C) = k$ is the set of customers assigned to the k-th table. Further, each marginal likelihood in (18) has the following form,

$$
p(\boldsymbol{\Xi}_{\mathbf{Z}(C)=k}|\lambda) = \int_{\theta}\left(\prod_{i\in\mathbf{Z}(C)=k} p\left(\boldsymbol{\xi}_i \mid \theta\right)\right) p\left(\theta \mid \lambda\right) d\theta. \tag{19}
$$

Since $p(\boldsymbol{\xi}_i \mid \theta) = \mathcal{N}(\boldsymbol{\xi}_i \mid \boldsymbol{\mu}, \boldsymbol{\Sigma})$ and $p(\theta \mid \lambda) = \mathcal{NIW}(\boldsymbol{\mu}, \boldsymbol{\Sigma} \mid \lambda)$, (19) has an analytical solution which can be derived from the posterior $p(\boldsymbol{\mu}, \boldsymbol{\Sigma}|\boldsymbol{\Xi})$ as presented in Appendix D.2.

D.2 Sampling from the $\mathcal{NIW}$ distribution

The $\mathcal{NIW}$ [28] is a four-parameter $\lambda = \{\mu_0, \kappa_0, \Lambda_0, \nu_0\}$ multivariate distribution generated by $\Sigma \sim \mathcal{IW}(\Lambda_0, \nu_0), \quad \mu|\Sigma \sim$ and $\mathcal{N}\left(\mu_0, \frac{1}{\kappa_0}\Sigma\right)$ where $\kappa_0, \nu_0 \in \mathbb{R}_{>0}$, and $\nu_0 > P - 1$ indicates degrees of freedom of the P-dimensional scale matrix $\Lambda \in \mathbb{R}^{PxP}$ which should be $\Lambda \succ 0$. The density of the $\mathcal{NIW}$ is defined by

$$\begin{aligned} p(\mu, \Sigma \mid \lambda) &= \mathcal{N}\left(\mu|\mu_0, \frac{1}{\kappa_0}\Sigma\right) \mathcal{IW}(\Sigma \mid \Lambda_0, \nu_0) \\ &= \frac{1}{Z_0}|\Sigma|^{-[(\nu_0+d)/2+1]} \exp\left\{-\frac{1}{2}\mathtt{tr}(\Sigma^{-1}\Lambda_0)\right\} \\ &\times \exp\left\{-\frac{\kappa_0}{2}(\mu-\mu_0)^T\Sigma^{-1}(\mu-\mu_0)\right\} \end{aligned} \tag{20}$$

where $Z_0 = \frac{2^{\nu_0 d/2}\Gamma_d(\nu_0/2)(2\pi/\kappa_0)^{d/2}}{|\Lambda_0|^{\nu_0/2}}$ is the normalization constant.

A sample from a $\mathcal{NIW}$ yields a mean μ and covariance matrix Σ. One first samples a matrix from an $\mathcal{W}^{-1}$ parameterized by Λ_0 and ν_0; then μ is sampled from a $\mathcal{N}$ parameterized by μ_0, κ_0, Σ. Since $\mathcal{N}$ and $\mathcal{NIW}$ are a conjugate pair, the term $\left(\prod_{i\in\mathbf{Z}(C)=k} p\left(\boldsymbol{\xi}_i \mid \theta\right)\right) p\left(\theta \mid \lambda\right)$ in (19) also follows a $\mathcal{NIW}$ [29] with new parameters $\lambda_n = \{\mu_n, \kappa_n, \Lambda_n, \nu_n\}$ computed via the following posterior update equations,

$$\begin{aligned} p(\mu, \Sigma|\boldsymbol{\Xi}_{1:n}, \lambda) &= \mathcal{NIW}(\mu, \Sigma|\mu_n, \kappa_n, \Lambda_n, \nu_n) \\ \kappa_n = \kappa_0 + n, \qquad \nu_n = \nu_0 + n, \qquad \mu_n &= \frac{\kappa_0\mu_0 + n\bar{\boldsymbol{\Xi}}}{\kappa_n} \\ \Lambda_n &= \Lambda_0 + S + \frac{\kappa_0 n}{\kappa_n}(\bar{\boldsymbol{\Xi}} - \mu_0)(\bar{\boldsymbol{\Xi}} - \mu_0)^T \end{aligned} \tag{21}$$

where N_k is the number of samples $\boldsymbol{\Xi}_{1:N_k}$, whose sample mean is denoted by $\bar{\boldsymbol{\Xi}}$ and $S = \sum_{i=1}^{N_k}(\boldsymbol{\xi}_i - \boldsymbol{\mu})(\boldsymbol{\xi}_i - \mu)^T$ is the matrix of sum of squares, otherwise known as the scatter matrix.

D.3 Collapsed Gibbs Sampler for Physically-Consistent Clustering

The conditional in (7) is sampled via a two-step procedure:

Step 1. The i-th customer assignment is removed from the current partition $\mathbf{Z}(C)$. If this causes a change in the partition; i.e. $\mathbf{Z}(C_{-i}) \neq \mathbf{Z}(C)$; the customers previously sitting at $\mathbf{Z}(c_i)$ are split and the likelihood must be updated via (18).

Step 2. A new customer assignment c_i must be sampled, by doing so a new partition $\mathbf{Z}(c_i = j \cup C_{-i})$ is generated. This new customer assignment might change (or not) the current partition $\mathbf{Z}(C_{-i})$. If $\mathbf{Z}(C_{-i}) = \mathbf{Z}(c_i = j \cup C_{-i})$, the partition was unchanged and the i-th customer either joined an existing table or sat alone. If $\mathbf{Z}(C_{-i}) \neq \mathbf{Z}(c_i = j \cup C_{-i})$, the partition was changed, specifically $c_i = j$ caused two tables to merge, table l which is where the i-th customer was sitting prior to step 1 and table m is the new table assignment emerged from the new sample $\mathbf{Z}(c_i = j)$. Due to these effects on the partition, instead of explicitly sampling from Eq. 7, [21] proposed to sample from the following distribution,

$$p(c_i = j \mid C_{-i}, \boldsymbol{\Xi}, \mathbf{S}, \alpha, \lambda) \propto \begin{cases} p(c_i = j|\mathbf{S}, \alpha)\Lambda(\boldsymbol{\Xi}, C, \lambda) & \text{if } \mathtt{cond} \\ p(c_i = j|\mathbf{S}, \alpha) & \text{otherwise,} \end{cases} \tag{22}$$

where $\mathtt{cond}$ is the condition of $c_i = j$ merges tables m and l and $\Lambda(\boldsymbol{\Xi}, C, \lambda)$ is equivalent to,

$$\Lambda(\boldsymbol{\Xi}, C, \lambda) = \frac{p(\boldsymbol{\Xi}_{(\mathbf{Z}(C)=m \cup \mathbf{Z}(C)=l)}|\lambda)}{p(\boldsymbol{\Xi}_{\mathbf{Z}(C)=m}|\lambda)p(\boldsymbol{\Xi}_{\mathbf{Z}(C)=l}|\lambda)}. \tag{23}$$

This procedure is iterated T times for a pre-defined number of iterations. The entire procedure is summarized in Algorithm 1.

Algorithm 1 Collapsed Gibbs Sampler for $\dot{\boldsymbol{\xi}}$-$\mathcal{SD}$-$\mathcal{CRP}$

Input: $\boldsymbol{\Xi}, \dot{\boldsymbol{\Xi}}$ ▷ Data
$\alpha, \lambda = \{\mu_0, \kappa_0, \Lambda_0, \nu_0\}$ ▷ Hyper-parameters
Output: $\Psi = \{K, C, Z, \Theta\}$ ▷ Inferred Clusters and Cluster indicators

Compute pair-wise $\dot{\boldsymbol{\xi}}$-similarity values (Eq.4)
procedure GIBBS-SAMPLER($\boldsymbol{\Xi}, \mathbf{S}, \alpha, \lambda$)
  Set $\Psi^{t-1} = \{C, K, Z\}$ where $c_i = i$ for $C = \{c_1, \ldots, c_N\}$
  for `iter t = 1 to T` **do**
    Sample a random perm. $\tau(\cdot)$ of integers $\{1, \ldots, N\}$.
    for `obs i =` $\tau(1)$ `to` $\tau(N)$ **do**
      Remove customer assignment c_i from the partition
      if $\mathbf{Z}(C_{-i}) \neq \mathbf{Z}(C)$ **then**
        Update likelihoods according to Eq. 18
      Sample new cluster assignment
      $c_i^{(i)} \sim p(c_i = j | C_{-i}, \boldsymbol{\Xi}_{-i}, \mathbf{S}, \alpha)$ (Eq. 22)
      if $\mathbf{Z}(C_{-i}) \neq \mathbf{Z}(c_i = j \cup C_{-i})$ **then**
        Update table assignments Z.
    Sample table parameters θ_γ from $\mathcal{NIW}$ posterior
      update equations (21).

E Further Illustrations and Comparisons for GMM Learning

Following we provide further comparison of the performance of the proposed GMM fitting approach on challenging datasets with characteristics specific to trajectory data.

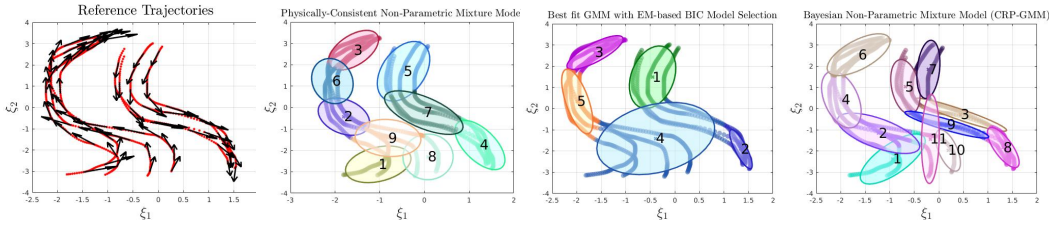

Figure 8: GMM fit on 2D Opposing Motions (Different Targets) Dataset.

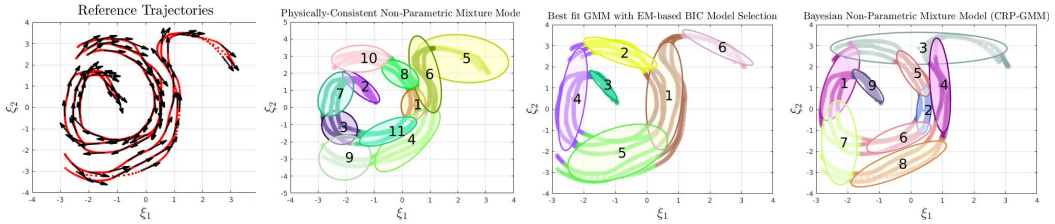

Figure 9: GMM fit on 2D Multiple Motions (Different Targets) Dataset.

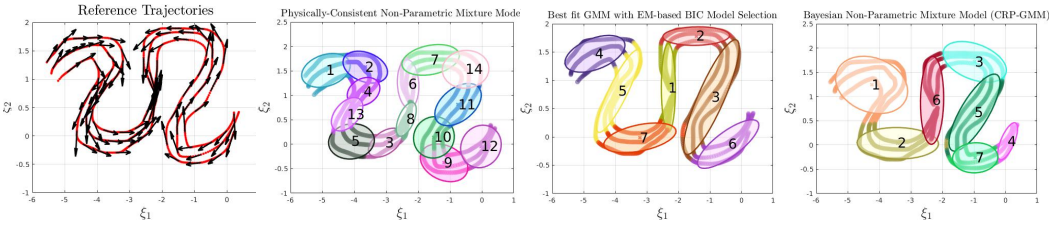

Figure 10: GMM fit on 2D Multiple Motions (Same Target) Dataset.

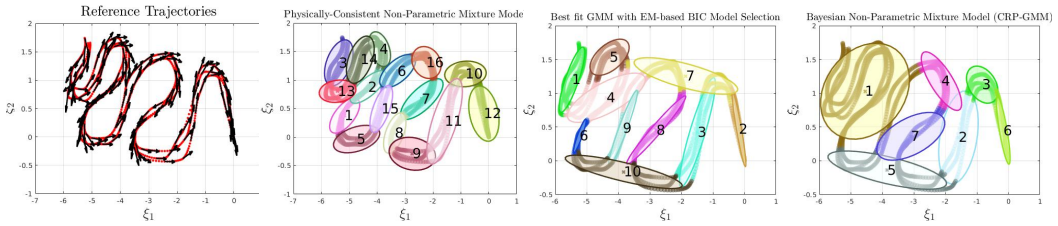

Figure 11: GMM fit on 2D Messy Snake Dataset.

F Stability of Merged DS $\tilde{\mathbf{f}}^{b+1}(\boldsymbol{\xi})$ for Incremental Learning Approach

We wish to prove Theorem 1 that is, that the merged DS $\tilde{\mathbf{f}}^{b+1}(\boldsymbol{\xi}) = \mathbf{f}^{b}(\boldsymbol{\xi}) \oplus \mathbf{f}^{b+1}(\boldsymbol{\xi})$ composed of individual DS (10) and (10) is globally asymptotically stable at the point $\boldsymbol{\xi}^*$ if there exists a continuous and continuously differentiable Lyapunov function $V(\boldsymbol{\xi}) : \mathbb{R}^N \to \mathbb{R}$ such that $V(\boldsymbol{\xi}) \succ 0, \dot{V}(\boldsymbol{\xi}) \prec 0 \; \forall \, \boldsymbol{\xi} \neq \boldsymbol{\xi}^*$ and $V(\boldsymbol{\xi}^*) = 0, \dot{V}(\boldsymbol{\xi}^*) = 0$. By considering a quadratic Lyapunov candidate function of the following form:

$$V(\boldsymbol{\xi}) = (\boldsymbol{\xi} - \boldsymbol{\xi}^*)^T (\boldsymbol{\xi} - \boldsymbol{\xi}^*) \tag{24}$$

we can ensure $V(\boldsymbol{\xi}) > 0$ due to its quadratic form. The second condition follows by taking the derivative of $V(\boldsymbol{\xi})$ wrt. time,

$$\begin{aligned}
\dot{V}(\boldsymbol{\xi}) &= \nabla_{\boldsymbol{\xi}} V(\boldsymbol{\xi})^T \frac{d}{dt}\boldsymbol{\xi}(t) = (\boldsymbol{\xi} - \boldsymbol{\xi}^*)^T \tilde{\mathbf{f}}^{b+1}(\boldsymbol{\xi}) \\
&= (\boldsymbol{\xi} - \boldsymbol{\xi}^*)^T \Big(\sum_{k=1}^{K^b} \gamma_k^b(\boldsymbol{\xi})(\mathbf{A}_k^b \boldsymbol{\xi} + \boldsymbol{b}_k^b) + \sum_{k=1}^{K^{b+1}} \gamma_k^{b+1}(\boldsymbol{\xi})(\mathbf{A}_k^{b+1} \boldsymbol{\xi} + \boldsymbol{b}_k^{b+1}) \Big) \\
&= (\boldsymbol{\xi} - \boldsymbol{\xi}^*)^T \Big(\sum_{k=1}^{K^b} \gamma_k^b(\boldsymbol{\xi}) \underbrace{(\mathbf{A}_k^b)(\boldsymbol{\xi} - \boldsymbol{\xi}^*)}_{\text{via (12)}} + \sum_{k=1}^{K^{b+1}} \gamma_k^{b+1}(\boldsymbol{\xi}) \underbrace{(\mathbf{A}_k^{b+1})(\boldsymbol{\xi} - \boldsymbol{\xi}^*)}_{\text{via (12)}} \Big) \\
&= (\boldsymbol{\xi} - \boldsymbol{\xi}^*)^T \Big(\sum_{k=1}^{K^b} \gamma_k^b(\boldsymbol{\xi}) \mathbf{A}_k^b + \sum_{k=1}^{K^{b+1}} \gamma_k^{b+1}(\boldsymbol{\xi}) \mathbf{A}_k^{b+1} \Big) (\boldsymbol{\xi} - \boldsymbol{\xi}^*) \\
&= (\boldsymbol{\xi} - \boldsymbol{\xi}_g^*)^T \Big(\underbrace{\sum_{k=1}^{K^b + K^{b+1}} \tilde{\gamma}_k^{b+1}(\boldsymbol{\xi})}_{>0 \text{ via (12)}} \underbrace{\left(\tilde{\mathbf{A}}_k^{b+1}\right)}_{\prec 0 \text{ via (12)}} \Big) (\boldsymbol{\xi} - \boldsymbol{\xi}_g^*) < 0
\end{aligned} \tag{25}$$

where $\sum_{k=1}^{K^b+K^{b+1}} \tilde{\gamma}_k^{b+1}(\boldsymbol{\xi}) = \sum_{k=1}^{K^b} \gamma_k^b(\boldsymbol{\xi}) + \sum_{k=1}^{K^{b+1}} \gamma_k^{b+1}(\boldsymbol{\xi})$ and $\tilde{\mathbf{A}}_k^{b+1}$ is the k-th matrix in the set of concatenated matrices $\tilde{\mathbf{A}}^{b+1} = \{\mathbf{A}_1^b, \ldots, \mathbf{A}_{K^b}^b, \mathbf{A}_1^{b+1}, \ldots, \mathbf{A}_{K^{b+1}}^{b+1}\}$. By substituting $\boldsymbol{\xi} = \boldsymbol{\xi}^*$ in (24) and (25) we ensure $V(\boldsymbol{\xi}^*) = 0, \dot{V}(\boldsymbol{\xi}^*) = 0$. Therefore, $\tilde{\mathbf{f}}^{b+1}(\boldsymbol{\xi})$ is globally asymptotically stable with respect to an attractor $\boldsymbol{\xi}^*$ if conditions (12) are satisfied.

G Further Results and Illustrations for DS Learning

G.1 Messy-snake dataset from Section x

In Figure 12 we show the resulting DS and Lyapunov functions from estimating an LPV-DS on the *messy-snake* dataset with the three optimization variants.

We further show more exemplars from the LASA Motion library and the computed performance metrics on training and testing sets in Figure 13, 14, 15.

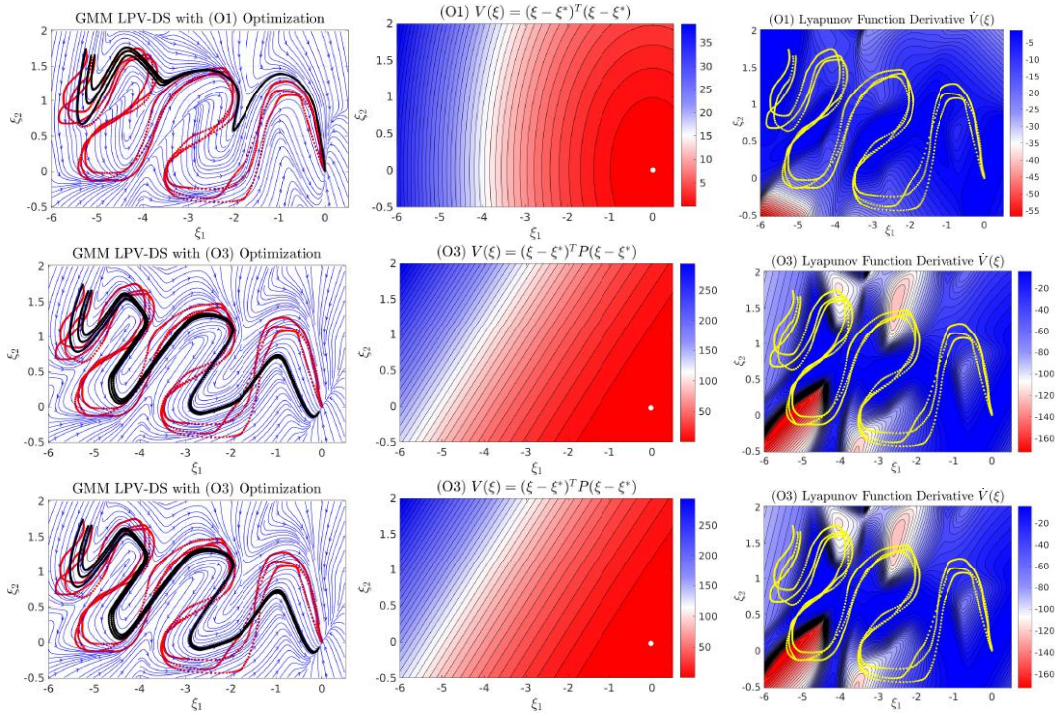

Figure 12: Illustrations of our physically-consistent GMM-based LPV-DS learning variants learned on the *messy-snake* dataset. Result of the optimization variant (9) **(1st row)** $(O1)$, **(2nd row)** $(O2)$ and **(2nd row)** $(O3)$.

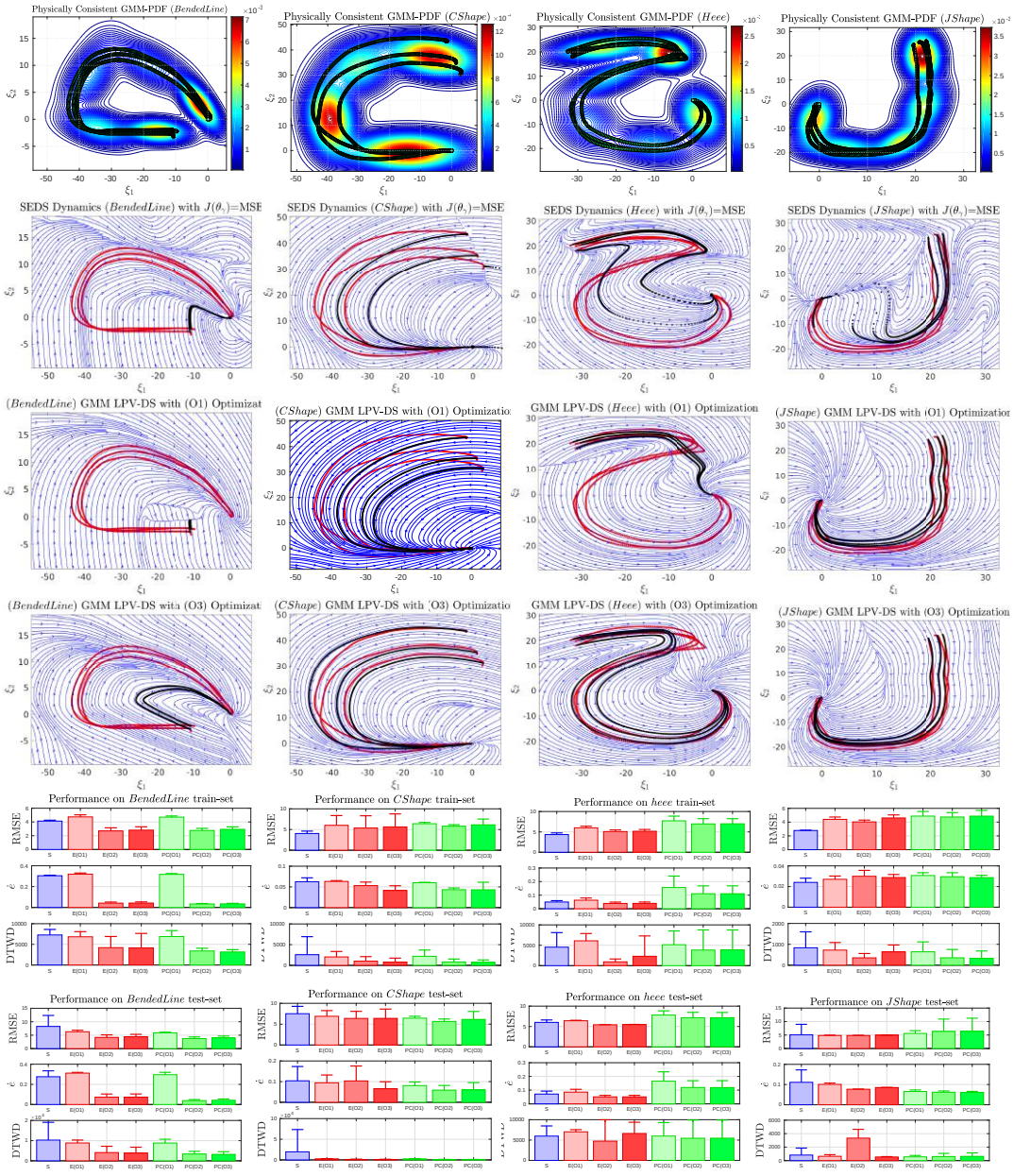

Figure 13: Exemplary models learned from the LASA handwriting dataset. **(1st row)** PDF of Physically-Consistent Mixture Model **(2nd row)** SEDS estimated with $J(\theta_\gamma)$=MSE **(3rd row)** GMM-based LPV-DS estimated via $(O1)$ **(4th row)** GMM-based LPV-DS estimated via $(O3)$. **(5th row)** Performance Metrics on Training set. **(5th row)** Performance Metrics on Testing set

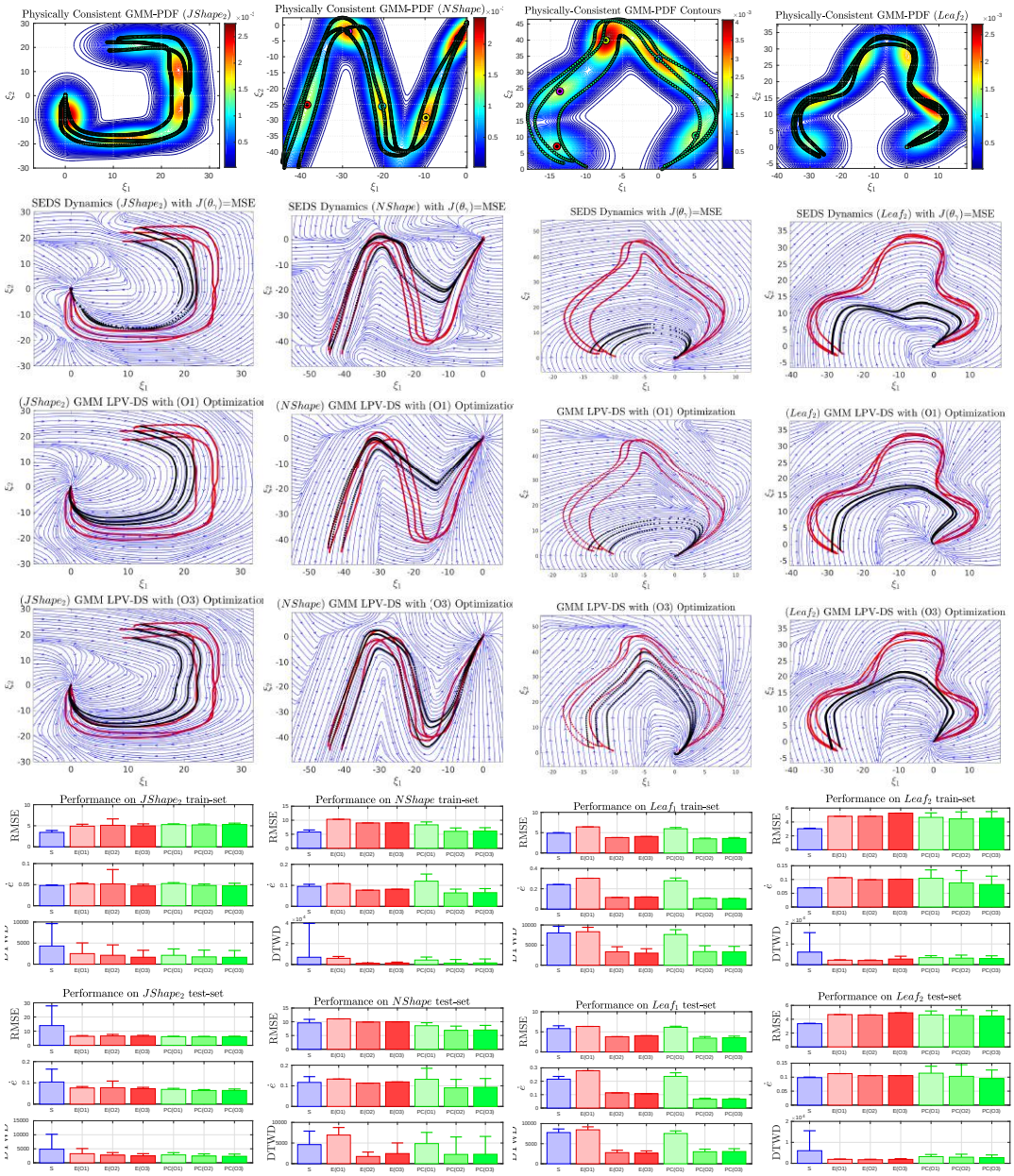

Figure 14: Exemplary models learned from the LASA handwriting dataset. **(1st row)** PDF of Physically-Consistent Mixture Model **(2nd row)** SEDS estimated with $J(\theta_\gamma)$=MSE **(3rd row)** GMM-based LPV-DS estimated via $(O1)$ **(4th row)** GMM-based LPV-DS estimated via $(O3)$. **(5th row)** Performance Metrics on Training set. **(5th row)** Performance Metrics on Testing set.

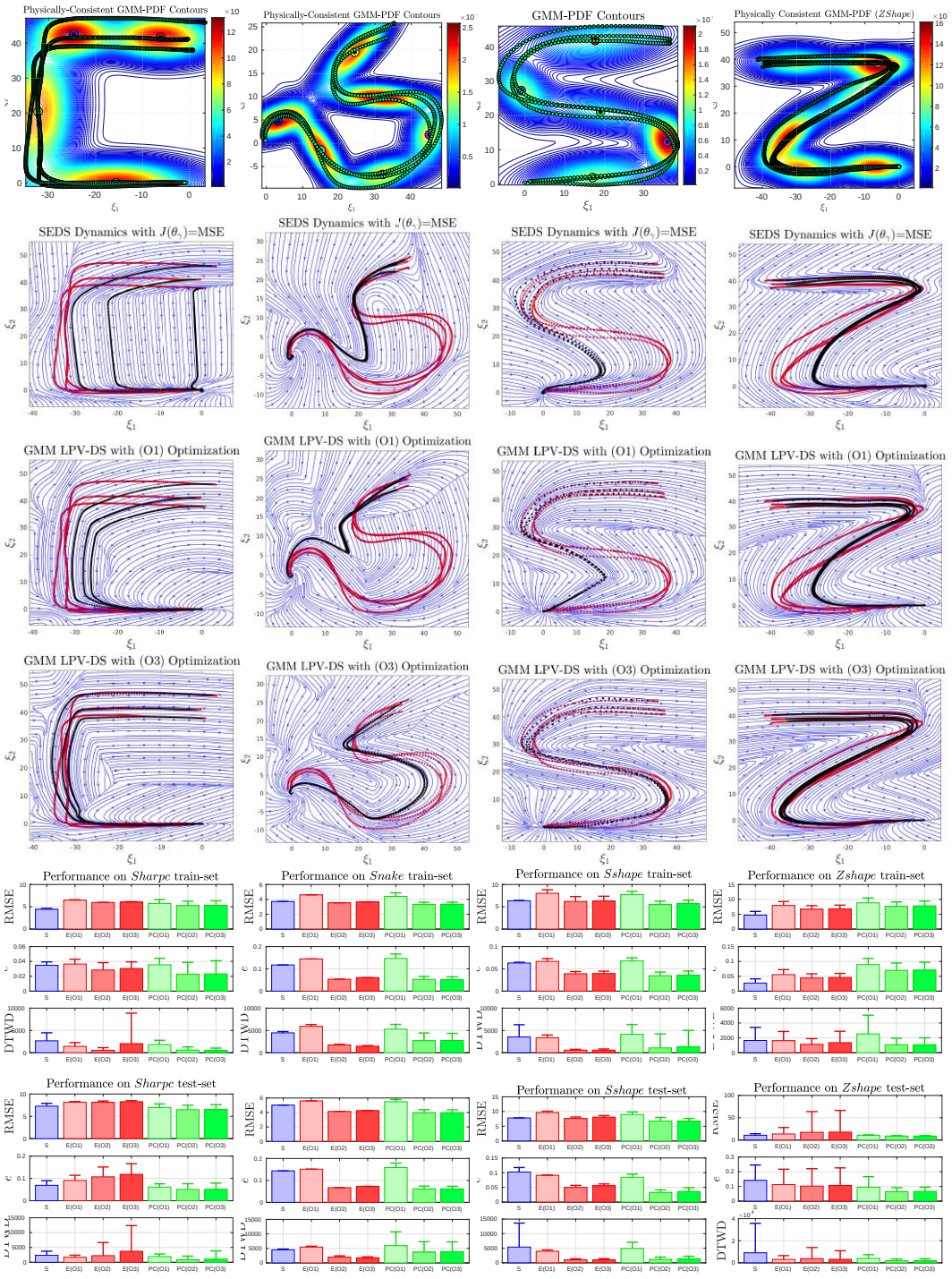

Figure 15: Exemplary models learned from the LASA handwriting dataset. **(1st row)** PDF of Physically-Consistent Mixture Model **(2nd row)** SEDS estimated with $J(\theta_\gamma)$=MSE **(3rd row)** GMM-based LPV-DS estimated via $(O1)$ **(4th row)** GMM-based LPV-DS estimated via $(O3)$. **(5th row)** Performance Metrics on Training set. **(5th row)** Performance Metrics on Testing set.

H Illustrations for Incremental Approach

Following we provide a second example for the incremental learning framework.

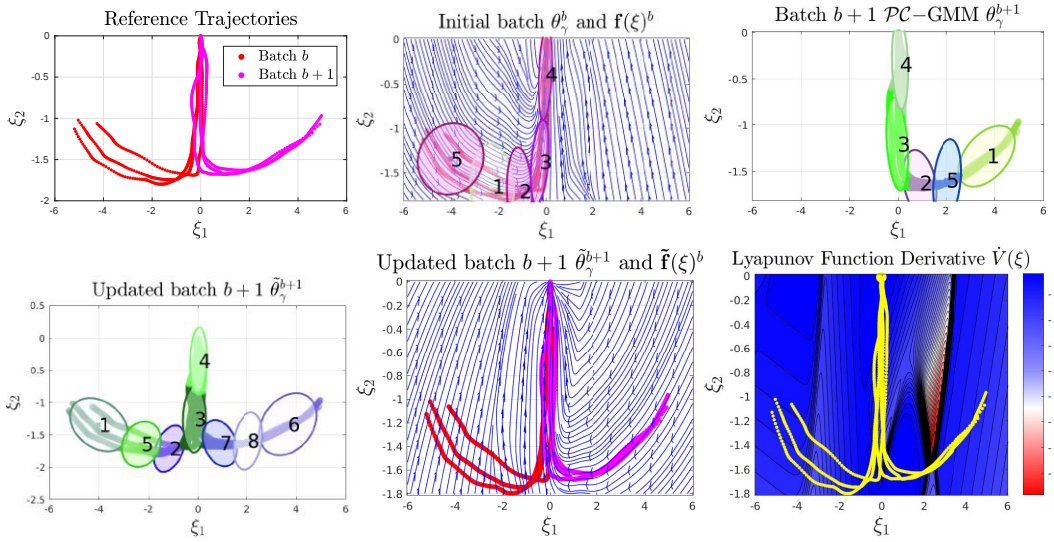

Figure 16: Illustration of Incremental $\mathcal{PC}$-GMM-based LPV-DS Learning Approach.